Absorption electronic spectrum of gaseous FeO: in situ detection with intracavity laser absorption spectroscopy in a nanoparticle-generating flame reactor

Igor Rahinov · Alexey Fomin · Marina Poliak · Sergey Cheskis

Abstract Absorption measurement of a gas-phase iron oxide (FeO) electronic spectrum is reported for the first time. FeO was obtained in a methane/oxygen/nitrogen flame doped with iron pentacarbonyl and monitored via the 611-nm band of the orange system with intracavity laser absorption spectroscopy. The measured spectral range extends from 16,250 to 16,450 cm^{-1} for the appropriate intracavity tuning element position. The presented measurements demonstrate sensitive detection of the gas-phase precursor, playing a key role in flame synthesis of iron oxide nanoparticles. The sensitivity of the intracavity technique does not depend on broadband cavity losses and allows conducting measurements in a highly scattering, particle-laden flame environment.

1 Introduction

Flame-assisted synthesis is an important route for production of high purity metal oxide nanoparticles with engineered functionalities, including particle size, morphology and chemical composition [1, 2]. Areas of metal oxides utilization range from telecommunication to heterogeneous catalysis. In this sense, the iron oxide nanoparticles are not exception: They are also used in gas sensing, catalysts, targeted drug delivery, etc. [3].

Production of the iron oxide nanoparticles with tailored properties by flame-assisted synthesis should rely on detailed understanding of the mechanisms governing their formation and nucleation from the gas phase. The chemistry of iron-containing gas-phase intermediates in the high-temperature flame environment is critical in establishing the final characteristics of the synthesized iron oxide nanoparticles. Quantitative in situ measurements of the concentration of gas-phase iron-containing intermediates are required for further development and validation of chemical mechanisms governing the precursor decomposition and particle formation. For example, quantitative measurements of Fe atoms in an H_2/O_2 flame doped with iron pentacarbonyl ($Fe(CO)_5$) conducted by Hecht et al. [4] enabled validation, updating and further development [5] of the $Fe(CO)_5$ reaction mechanism previously proposed by Rumminger et al. [6]. Clearly, additional quantitative measurements of gas-phase iron-containing intermediate targets (such as FeO), against which the mechanism can be validated and improved, are required. Moreover, flames doped with $Fe(CO)_5$ are sensitive to the presence of iron-containing species, and, in particular, FeO is intimately related to the fire-suppressing properties of iron-containing compounds, as it reacts in a catalytic cycle with flame carrier radicals and atoms (e.g., H and OH) [6]. The interest in FeO extends beyond the role it plays in combustion synthesis of iron oxide nanoparticles and fire suppression: A great deal of studies have been devoted to the iron monoxide molecule, motivated by its chemical importance and complicated electronic states structure [7–21]. A considerable and impressive effort, employing laser induced fluorescence (LIF), was directed toward spectroscopic studies of FeO in the orange region, aiming to study the features of its extraordinarily complex

I. Rahinov (✉)
Department of Natural Sciences, The Open University of Israel, Raanana 4353701, Israel
e-mail: igorra@openu.ac.il

A. Fomin · M. Poliak · S. Cheskis
School of Chemistry, Tel Aviv University, Tel Aviv 69978, Israel

Fig. 1 A schematic of the experimental setup for ICLAS measurements in a nanoparticle flame reactor. The pumping laser beam (frequency doubled output of an Nd–YAG laser) is focused on the dye jet by mirror M3. The homebuilt dye laser cavity is formed by mirrors M1, M2 and OC (output coupler). AOM1 and AOM2 are acousto-optic modulators. CCD—is a charge coupled device. PBS—is a pellicle beam splitter
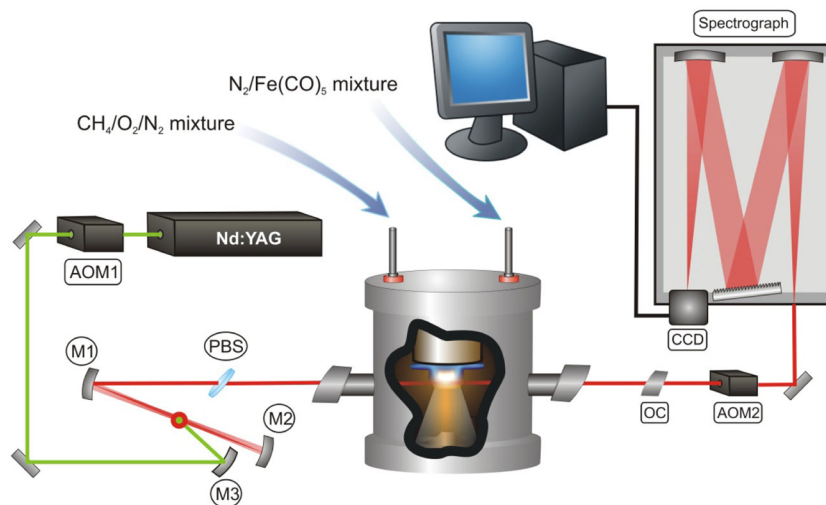
electronic spectrum, which, to date, has not been fully understood [11–14]. Despite the considerable body of studies devoted to spectroscopic detection of FeO, the work of McMillin et al. [10] is, perhaps, the only one, where laser-based detection and semi-quantitative spatial distributions of FeO in the nanoparticle flame reactor were reported. LIF detection used in [10] faces challenges associated with the need to record the resonant fluorescence signal on top of a broadband background originating from increased flame luminosity and laser light scattering, characteristic for particle-laden environments. The authors of this work report that in order to avoid corrupting the FeO fluorescence signal with extraneous noise (light scattering and flame luminosity), spectral filtering was necessary, which inevitably lead to a reduction of over 50 % in the signature fluorescence signal. Absorption spectroscopy techniques have developed during the last couple of decades to offer a useful complement and, sometimes, powerful alternative to LIF in cases where absolute calibration is required or where detection of fluorescence signal is hampered by collisional quenching, pre-dissociation or strong background luminosity (see for example Ref [22] and references therein). In this respect, cavity ring-down spectroscopy (CRDS) [23–27] (with the absorber placed inside a passive high finesse cavity) and intracavity laser absorption spectroscopy (ICLAS) [28–33] (with the absorber placed inside the laser cavity) have matured to be the most powerful and robust. In the present work, ICLAS was applied for FeO monitoring in methane/oxygen flames doped with $Fe(CO)_5$. To the best of our knowledge, this is the first time that the electronic spectrum of FeO is monitored in absorption. In this particle-laden environment, ICLAS has an important advantage over CRDS: In ICLAS, the laser gain compensates broadband cavity losses (such as scattering due

solid particulates), but not the narrowband intracavity absorption.

2 Experimental

The experimental apparatus used in this work has been described previously [31, 34–36], so only an overview will be presented here. The experimental apparatus including the low-pressure nanoparticle flame reactor and the ICLAS optical layout is shown in Fig. 1.

2.1 Nanoparticle-generating flame reactor

The flame reactor houses a modified McKenna flat flame burner, including a water-cooled bronze-porous plug with a 60-mm diameter on which a stoichiometric methane (450 sccm)/oxygen (900 sccm)/nitrogen (2,300 sccm) primary flame is stabilized. The gases forming the primary flame are supplied via calibrated mass flow controllers (MKS Instruments). A secondary methane(100 sccm)/oxygen(70 sccm) flame is stabilized on a coaxial narrow central tube (4.2 mm I.D.). Fuel (methane), oxidizer (oxygen) and precursor (1–40 sccm of 1 % $Fe(CO)_5$) vapors diluted in N_2, corresponding to 60–2,370 ppm precursor load in the secondary flame are supplied separately to the central tube via calibrated mass flow controllers (MKS Instruments). The burner is mounted such that the gases propagate from top to bottom. The burner is translated along the vertical coordinate with the aid of a stepper motor (Huntington Labs, model I-2252-8 controlled by Thorlabs controller BSC101, 0.1 mm accuracy). The total pressure in the reactor chamber is kept at 30 Torr with the aid of a feedback valve controller (model 252/253 MKS Instruments) equipped with an exhaust throttle valve.

2.2 ICLAS optical layout

The nanoparticle synthesis flame reactor is placed inside the cavity of a homebuilt quasi-cw dye-jet laser and is isolated from other parts of the cavity by two glass windows placed at Brewster's angle (see Fig. 1). The widows are slightly wedged (1° divergence) to minimize interference fringes in the spectrum. The laser consists of the dye jet placed inside an astigmatically compensated, three-mirror folded cavity formed by M1, M2 and OC (output coupler). The central wavelength of this broadband laser source can be tuned by introducing a thin pellicle beamsplitter (BP108, Thorlabs) inside the cavity. Kiton Red dye dissolved in ethylene glycol was used in this work. The dye jet is pumped by a focused (with the aid of mirror M3) 532 nm laser beam produced by an Nd–YAG laser with intracavity doubling (SPROUT, Lighthouse Photonics). The laser generation time t_g, in the ICLAS is the time interval between the beginning of the laser generation and the sampling, which is related to the effective pathlength of the laser beam through the sample via the following straightforward expression [28–30]:

$$L_{\text{eff}} = \frac{c t_g l}{L} \tag{1}$$

where c is the speed of light, l is the sample length (~ 2 cm in our case) and L is the length of the cavity (90 cm in our case). The generation time $t_g = 25$ μs used in our experiments corresponds to the effective pathlength $L_{\text{eff}} = 166$ m. The generation time is controlled with the aid of two acousto-optical modulators (AOM), synchronized by a pulse/delay generator (Model 555, Berkeley Nucleonics). The first modulator, AOM1, (AFM-402 IntraAction Corp.) chops the 532 nm Nd–YAG laser beam and produces laser pulses with a controlled duration (30 μs) and high repetition rate (25 kHz in our case). After a delay $t_g = 25$ μs from the beginning of each AOM1 pulse, the second modulator, AOM2 (AOM-40 IntraAction Corp.), delivers the laser beam (during the sampling time of 5 μs) to the entrance slit of the high resolution 1-m spectrograph (SPEX 1000M), where the dye laser output is dispersed by the 100 grooves/mm echelle grating. The width of the dye laser spectral profile allows to work at the 29th order of diffraction without overlapping with adjacent orders. The spectrally dispersed laser output is recorded with a 3,648 pixel CCD line camera (TCE-1304-UW, Mightex Systems). The monochromator dispersion is ~ 0.03 cm^{-1} per pixel of the CCD camera. Information from the CCD is stored and processed on a computer. The exposure time of the CCD is set to 0.3 s, corresponding to averaging of 7500 ICLAS spectra. In addition, 10–50 CCD traces were averaged on the computer.

3 Results and discussion

The fuel-rich hybrid methane/oxygen/nitrogen flame used in this work is shown in Fig. 2c. Once the iron pentacarbonyl precursor is added, strong yellow luminosity originating from blackbody radiation of iron oxide nanoparticles and chemiluminescence of electronically excited FeO is readily observed by the naked eye—see Fig. 2d. The electronic spectrum of the FeO orange system consists of irregular bands covering the range of 530–650 nm [11, 12]. In this work, we monitored FeO in the 611-nm band range. In the absence of iron pentacarbonyl, the laser spectrum in the 611-nm range contains HCO and $^1CH_2$ spectral features (most prominently at 3–4 mm from the burner, near the primary flame front). The presence of HCO and $^1CH_2$ spectral lines in this spectral range was utilized for the spectrograph calibration. Spectra without the addition of Fe(CO)$_5$ (see Fig. 2a showing the envelopes of laser generation for several positions of the pellicle beamsplitter) were recorded at each set of measurement conditions and served as analogs of a "blank" spectra, $I_0(v)$, in conventional absorption spectroscopy. With the addition of iron pentacarbonyl precursor, narrowband absorption features characteristic to the FeO orange system, $I(v)$, appeared on top of the broadband dye laser envelopes (Fig. 2b). These spectral features appear only upon addition of iron pentacarbonyl. A typical ICLAS spectrum at $t_g = 25$ μs, and a single position of the pellicle beam splitter has a width of ~ 50 cm^{-1}. By tilting the pellicle beam splitter inside the dye-jet laser cavity, the spectral position of the center of the laser generation envelope was varied within a tuning range of ~ 200 cm^{-1}, see Fig. 2a,b.

The absorbance spectrum of the 611-nm band belonging to the FeO orange system, within a 200 cm^{-1} range (Fig. 3), was obtained by normalizing the ICLAS spectra containing the FeO spectral signature (Fig. 2b) by the spectra recorded without the iron-containing precursor (Fig. 2a). Therefore, spectra, such as the one shown in Fig. 3, contain only features originating from iron pentacarbonyl addition.

The FeO electronic spectrum possesses complexity almost unparalleled for a diatomic molecule. This is due to the fact that the orange system is a strongly perturbed $^5\Delta_i - ^5\Delta_i$ electronic transition, where the upper $^5\Delta$ state is subject to massive spin and rotational perturbations by a host of levels $v > 0$ and B values ranging from 0.38 to 0.50 cm^{-1} [11–13]. In a flame environment, this spectrum is further complicated, since FeO has a number of low-lying vibrational and electronic states that are significantly populated at flame temperatures. The 611-nm band of the orange system (Fig. 3) originates from the $(\Omega' = \Omega'' = 4, v'' = 0)$ transition. The upper level of the 611-nm band
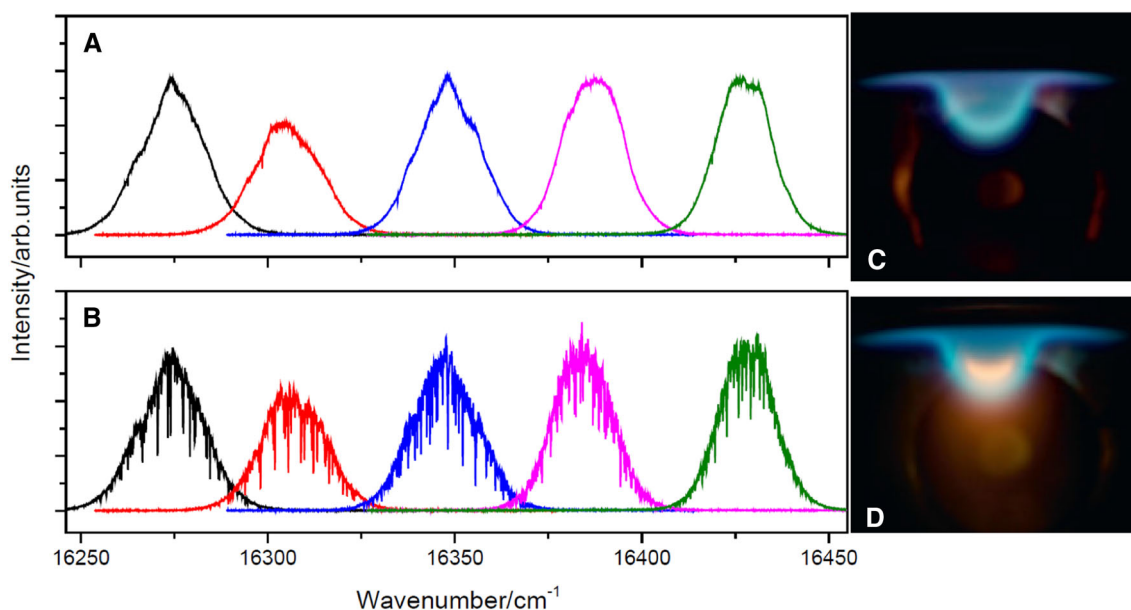
Fig. 2 **a** Dye-jet laser generation spectral profile, $I_0(v)$, recorded for various positions of the pellicle beam splitter at ~ 13 mm from the burner in the fuel-rich $CH_4/O_2/N_2$ flame without iron pentacarbonyl (the visual appearance of the flame is shown in **c**); **b** dye-jet laser generation spectral profile, $I(v)$, recorded for various positions of the pellicle beam splitter at ~ 13 mm from the burner in the fuel-rich $CH_4/O_2/N_2$ flame after the addition of 545 ppm of iron pentacarbonyl (the visual appearance of the flame is shown in **d**)
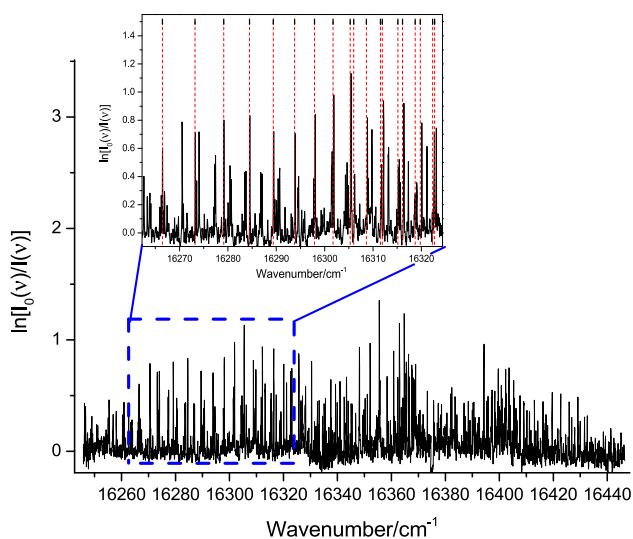

Fig. 3 Absorbance spectrum of the FeO orange system obtained by the combination of spectra corresponding to the individual pellicle positions shown in Fig. 2a, b. *Insert* zoomed-in portion of the spectrum with assignment of some of the lines belonging to the P-branch of the $(\Omega' = \Omega' = 4, v'' = 0)$ transition

has two large avoided crossings, reducing the branch structure to a highly irregular spectral pattern [12, 13]. The inset in Fig. 3 shows a zoomed-in portion of the 611-nm band of the FeO orange system with assignment of the most prominent P-branch lines of the $(\Omega' = \Omega'' = 4, v'' = 0)$ transition based on the analysis of Cheung et al. [12].

The FeO spectrum shown in Fig. 3 was recorded in the flame doped with 545 ppm of iron pentacarbonyl precursor. A signal-to-noise ratio as high as ~ 30 was observed under our measurement conditions. We found that the measured iron oxide absorbance signal depends linearly on the pentacarbonyl precursor load in the unburnt gas mixture. It implies that FeO would be detectable for iron pentacarbonyl concentrations as low as 20 ppm. Experimentally, we could observe FeO in flames with precursor loads as low as 60 ppm, as a result of the limitations induced by the mass flow controller rather than detection sensitivity. Zachariah and coworkers [10] who detected FeO in flame by LIF via the 558 nm band of the orange system were using 172–825 ppm iron pentacarbonyl precursor loads. Taking into account the relative intensity of the 558- and 611-nm bands [15], monitoring of 611-nm band would require precursor loads of ~ 690–3,300 ppm to maintain a similar signal-to-noise ratio, all other factors being equal under their LIF measurement conditions. An additional sensitivity enhancement can be reached by an increase of the effective path length. It can be done both by increasing the l/L ratio, which is only 2/90 under current conditions, and by increasing t_g. Note that in the dye laser-based system, the sensitivity was found to increase linearly (according to Eq. (1)) up to 0.4 ms even in the flame environment [22].

Unfortunately, the literature is lacking data on quantum-state-specific absorption cross-sections of the FeO orange system transitions, required to deduce the

absolute concentration. The reason for that is the absence, to date, of absorption spectroscopy measurements of FeO under conditions of known concentration (e.g., by means of controlled photolysis or pyrolysis experiments [37]). On the other hand, the very complex electronic spectrum of FeO makes the recalculation of the absorption cross-section from rotational-quantum-state-resolved fluorescence lifetimes (e.g., the way it was done for the $^{1}CH_2$ radical [38]) extremely difficult (see analogous problem for CrO absorption spectra [39]). Note that even without this knowledge, the absorbance signal derived from ICLAS measurements allows us to faithfully map the FeO concentration in relative units, since no knowledge of the fluorescence quantum yield and its dependence on the flame conditions (necessary for deducing the relative concentration from the LIF signal) is required. On the other hand, ICLAS, as any absorption technique, does not allow to resolve the concentration distribution along the line-of-sight, and the measurement outcome is essentially a path-integrated result. LIF, on the other hand, does possess the advantage of spatial resolution along the laser beam. In combination with Planar-LIF (PLIF), ICLAS can potentially provide a method for spatially resolved measurements of FeO relative (and with the knowledge of absorption coefficients even absolute) spatially resolved (along the laser beam) concentration profiles [27].

The ICLAS is insensitive to broadband light extinction induced by particle scattering: no increase of the noise level was observed in FeO spectra recorded at higher precursor loads (as high as $\sim 2{,}400$ ppm), even where the beam scattering on iron oxide nanoparticles in the combustion chamber could be vividly observed by the naked eye. Moreover, the threshold pumping power of the Nd–YAG laser required for the dye-jet laser operation has not changed upon increasing of the particle load. Note that ICLAS, in principle, permits recording of narrowband absorption spectra, while off-resonant broadband losses reach values as high as $\sim 5~\%$ per pass.

The FeO absorbance can be deduced using individual lines of ICLAS spectra or, with better accuracy, by taking into account several spectral lines employing a fitting procedure proposed by Bryukov et al. [40], and previously used by us for the deconvolution of the CN radical spectrum, superimposed with an intense spectrum of NH_2 [41] and for evaluation of relative concentrations of the HSO radical [32]. In this fitting procedure, the experimental dye laser spectrum $I_{exp}(v)$, is approximated by a broadband Gaussian envelope multiplied by a narrowband transmission function, representing the spectra of absorbing molecules. Therefore, the logarithm of the experimental laser spectrum can be represented as follows:

$$\ln\left[I_{exp}(v)\right] = P^{(m)} + n_{exp}k(v) + r(v) \qquad (2)$$

where $P^{(m)}$ is an m-order polynomial representing the spectral envelope, $k(v) = \sigma(v)L_{eff}$ is the spectrum of the species of interest (where $\sigma(v)$ is the absorption cross-section and L_{eff} is the effective pathlength of the laser beam through the sample given by Eq. (1)) and $r(v)$ is a residual usually consisting of "white" noise. When the spectrum $k(v)$ is known, the concentration n can be determined using a linear least squares fit method to experimental data. Instead of $k(v)$, one of the experimental ICLAS spectra, containing both the envelope $P^{(m)}$ and the $k(v)$, can be used. Such experimental ICLAS spectrum serves as a *reference spectrum*, $I_{ref}(v)$. Here, the FeO spectrum recorded at ~ 13 mm from the burner in a flame doped with 545 ppm of iron pentacarbonyl served as $I_{ref}(v)$. We applied the above described fitting procedure to all other spectra, $I_{exp}(v)$, (recorded at different distances from the burner and/or different dopant concentrations) to extract the relative concentration $n = n_{exp}/n_{ref}$. The spectrum $k(v)$ in ICLAS consists of very narrow lines and, therefore, cannot be expressed as a linear combination of low-order polynomials; thus, the order of the polynomial $P^{(m)}$ ($m = 5$–7) does not substantially affect the resulting value n extracted from the fit of the logarithm of the ICLAS spectrum to Eq. (2). Moreover, the experimental ICLAS spectrum, $I_{exp}(v)$, can contain any smooth baseline, which can be approximated by low-order polynomials. Only the polynomial coefficients obtained by the least squares fitting procedure will vary without significantly altering the extracted n value. This means that the above described fitting procedure enables to make an adequate background correction when scattering and other broadband background light extinction is present simultaneously with the narrow absorption dips during particle synthesis. If the relative intensities in the spectrum are changed in comparison with the reference spectrum, it will be reflected in the residual. We observed no variation in the intensity ratio between different spectral lines of FeO within the temperature range in the locations where FeO is present, due to a relatively low rotational constant of the iron oxide molecule. Furthermore, using the fitting procedure enables to simultaneously account for multiple lines, including strong and overlapped ones (especially relevant to the very dense and irregular FeO spectrum), allowing to reduce the random noise in the measured absorbance profiles. Such a profile is shown in Fig. 4. This absorbance profile can be, to a certain extent, considered a relative line-of-sight-integrated concentration profile, assuming weak variations of the temperature and absorption pathlength. The precursor oxidation (FeO formation) and iron oxide particulates formation (FeO consumption) are simultaneously taking
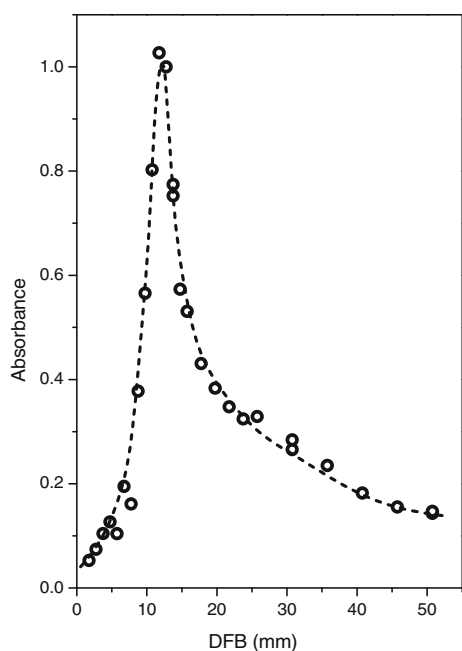
Fig. 4 Absorbance profile of FeO in a rich methane/oxygen flame doped with 545 ppm of iron pentacarbonyl. The *empty circles* are the experimental data. The *dashed line* is drawn to guide the eye through the experimental data points. DFB is the distance from the burner

place, giving rise to a profile with a sharp maximum at ~ 13 mm from the burner. Note that the hybrid flame used in this work is not flat, and one has to be cautious making conclusions about FeO consumption and formation kinetics based on the path-integrated absorption measurements. While further study, including flat flame configuration and/ or measurements resolving FeO concentration along the laser beam are required, the presented result clearly shows that ICLAS is a compelling method for monitoring FeO concentrations in a particle-laden flame environment. In combination with PLIF [10, 27] or using tomographic reconstruction [42], it can contribute to quantitative understanding of the particle formation kinetics in flat-flame and more complicated configurations of the particle synthesis reactor. This work is currently underway in our laboratory.

4 Conclusions

In summary, the orange system electronic spectrum of FeO was monitored for the first time in absorption via the 611-nm band, by ICLAS. The detection was performed under flame conditions complicated by the presence of a heavy load of solid particulates present in the nanoparticle flame reactor. No decrease of the detection sensitivity was observed, due to the insensitivity of ICLAS to broadband light attenuation. The method demonstrated in this work for FeO can be applied for other molecular species in the

visible and near infrared range in the presence of heavy particle loads and can serve as a useful complementation to the spatially resolved fluorescence based methods, such as PLIF. We hope that this work will stimulate further detailed validation with flame kinetic modeling to better understand flame-assisted nanoparticle synthesis.

References

1. W.Y. Teoh, R. Amal, L. Madler, Nanoscale **2**(8), 1324 (2010)
2. P. Roth, Proc. Combust. Inst. **31**, 1773 (2007)
3. A.H. Lu, E.L. Salabas, F. Schuth, Angew. Chem. Int. Edit. **46**(8), 1222 (2007)
4. C. Hecht, H. Kronemayer, T. Dreier, H. Wiggers, C. Schulz, Appl. Phys. B Lasers Opt. **94**(1), 119 (2009)
5. I. Wlokas, A. Faccinetto, B. Tribalet, C. Schulz, A. Kempf, Int. J. Chem. Kinet. **45**(8), 487 (2013)
6. M.D. Rumminger, D. Reinelt, V. Babushok, G.T. Linteris, Combust. Flame **116**(1–2), 207 (1999)
7. R.J. Rollason, J.M.C. Plane, PCCP Phys. Chem. Chem. Phys. **2**(10), 2335 (2000)
8. R.S. Furuya, C.M. Walmsley, K. Nakanishi, P. Schilke, R. Bachiller, Astron. Astrophys. **409**(2), L21 (2003)
9. C.M. Walmsley, R. Bachiller, G.P. Des Forets, P. Schilke, Astrophys. J. **566**(2), L109 (2002)
10. B.K. McMillin, P. Biswas, M.R. Zachariah, J. Mater. Res. **11**(6), 1552 (1996)
11. A.S.C. Cheung, N. Lee, A.M. Lyyra, A.J. Merer, A.W. Taylor, J. Mol. Spectrosc. **95**(1), 213 (1982)
12. A.S.C. Cheung, A.M. Lyyra, A.J. Merer, A.W. Taylor, J. Mol. Spectrosc. **102**(1), 224 (1983)
13. M. Barnes, M.M. Fraser, P.G. Hajigeorgiou, A.J. Merer, J. Mol. Spectrosc. **170**(2), 449 (1995)
14. S.M. Harris, R.F. Barrow, J. Mol. Spectrosc. **84**(2), 334 (1980)
15. H.S. Son, K. Lee, S.K. Shin, J.K. Ku, Chem. Phys. Lett. **320**(5–6), 658 (2000)
16. I. Banerjee, N.K. Joshi, S.N. Sahasrabudhe, N.V. Kulkarni, S. Karmakar, R. Pasricha, S. Ghorui, A.K. Tak, S. Murthy, S.V. Bhoraskar, A.K. Das, IEEE Trans. Plasma Sci. **34**(4), 1175 (2006)
17. M.D. Allen, L.M. Ziurys, J.M. Brown, Chem. Phys. Lett. **257**(1–2), 130 (1996)
18. J.B. West, H.P. Broida, J. Chem. Phys. **62**(7), 2566 (1975)
19. J.B. West, H.P. Broida, IEEE J. Quantum Electron. **11**(8), 692 (1975)
20. G.V. Chertihin, W. Saffel, J.T. Yustein, L. Andrews, M. Neurock, A. Ricca, C.W. Bauschlicher, J. Phys. Chem. **100**(13), 5261 (1996)
21. D.W. Green, G.T. Reedy, J.G. Kay, J. Mol. Spectrosc. **78**(2), 257 (1979)
22. S. Cheskis, A. Goldman, Prog. Energy Combust. Sci. **35**(4), 365 (2009)
23. A. O'Keefe, D.A.G. Deacon, Rev. Sci. Instrum. **59**(12), 2544 (1988)
24. D. Romanini, K.K. Lehmann, J. Chem. Phys. **99**(9), 6287 (1993)
25. A. Schocker, K. Kohse-Hoinghaus, A. Brockhinke, Appl. Opt. **44**(31), 6660 (2005)

26. J.J. Scherer, D.J. Rakestraw, Chem. Phys. Lett. **265**(1–2), 169 (1997)
27. J. Luque, P.A. Berg, J.B. Jeffries, G.P. Smith, D.R. Crosley, J.J. Scherer, Appl. Phys. B Lasers Opt. **78**(1), 93 (2004)
28. V.M. Baev, T. Latz, P.E. Toschek, Appl. Phys. B Lasers Opt. **69**(3), 171 (1999)
29. A. Campargue, F. Stoeckel, M. Chenevier, Spectrochimica Acta Rev. **13**(1), 69 (1990)
30. I. Rahinov, N. Ditzian, A. Goldman, S. Cheskis, Proc. Combust. Inst. **30**, 1575 (2005)
31. A. Goldman, S. Cheskis, Appl. Phys. B Lasers Opt. **92**(2), 281 (2008)
32. I. Rahinov, A. Goldman, S. Cheskis, Isr. J. Chem. **47**(2), 131 (2007)
33. S.J. Harris, Appl. Opt. **23**(9), 1311 (1984)
34. A. Fomin, M. Poliak, I. Rahinov, V. Tsionsky, S. Cheskis, Combust. Flame **160**(10), 2131 (2013)

35. A. Hevroni, H. Golan, A. Fialkov, I. Rahinov, V. Tsionsky, G. Markovich, S. Cheskis, Meas. Sci. Technol. **22**(11), 115102 (2011)
36. I. Rahinov, A. Goldman, S. Cheskis, Appl. Phys. B Lasers Opt. **81**(1), 143 (2005)
37. K. Kohse-Hoinghaus, D.F. Davidson, A.Y. Chang, R.K. Hanson, J. Quant. Spectrosc. Radiat. Transf. **42**(1), 1 (1989)
38. I. Derzy, V.A. Lozovsky, S. Cheskis, Chem. Phys. Lett. **313**(1–2), 121 (1999)
39. B.P. Wilcox, E.T.H. Chrysostom, A. McIlroy, J.W. Daily, I.M. Kennedy, Appl. Phys. B Lasers Opt. **77**(5), 535 (2003)
40. M.G. Bryukov, A.A. Kachanov, S.I. Panov, O.M. Sarkisov, J. Phys. IV **1**(C7), 485 (1991)
41. I. Rahinov, N. Ditzian, V.A. Lozovsky, S. Cheskis, Chem. Phys. Lett. **352**(3–4), 169 (2002)
42. I. Rahinov, A. Goldman, S. Cheskis, Combust. Flame **145**(1–2), 105 (2006)